Int. J. Solids Structures Vol. 27, No. 8, pp. 949–964, 1991
Printed in Great Britain.

0020–7683/91 $3.00 + .00

REFLECTION OF PLANE STRAIN WAVES AT THE FREE EDGE OF A LAMINATED COMPOSITE PLATE

W. M. KARUNASENA and A. H. SHAH
Department of Civil Engineering, University of Manitoba, Winnipeg, Manitoba, Canada R3T 2N2

and

S. K. DATTA
Department of Mechanical Engineering and CIRES, University of Colorado, Boulder, CO 80309, U.S.A.

(*Received* 12 *November* 1989; *in revised form* 30 *March* 1990)

Abstract—A wave function expansion method has been used to solve the problem of reflection of time-harmonic plane strain waves normally incident upon the free edge of a semi-infinite, laminated orthotropic plate of linearly elastic materials. Both symmetric and antisymmeric incident waves have been considered. The exact dispersion relation of the laminated infinite plate is solved numerically by using Muller's method, with initial guesses obtained through an approximate technique. Propagator matrices are employed to obtain wave functions. It is illustrated that the least-squares method yields anomalous results. Numerical results using the variational method are presented for a single-layered graphite/epoxy (transversely isotropic) plate and for a 35-layer cross-ply (90°/0°/.../90°/0°/90°/.../0°/90°), laminated composite graphite/epoxy plate. In each case, the division of energy among various reflected modes is determined. The end resonance for the single layer graphite/epoxy plate is also reported.

1. INTRODUCTION

Wave scattering due to inhomogeneities in plates has been a subject of research interest for the past few years. A comprehensive knowledge of wave scattering plays an important role in identifying planar cracks in plates. One approach to solve the wave scattering problem is to represent the scattered field by wave function expansion, as reported by Abduljabbar *et al.* (1983) for horizontally polarized shear wave diffraction by normal edge cracks in an isotropic plate. The free edge of a plate can be considered as a through-thickness crack which is a special case of an inhomogeneity. The study of wave reflection at the free edge of a laminated composite plate will help in devising suitable techniques to analyse the more complicated problem of wave scattering due to cracks in composite plates. The present study of reflection of plane strain waves at the free edge of a laminated composite plate has been motivated by these reasons.

In order to represent the reflected wave field by the wave function (eigenfunction) expansion, displacement and stress eigenfunctions at the frequency range of interest have to be established. Computation of the eigenfunctions is straightforward if, for a given frequency, the eigenvalues (wavenumbers) of the dispersion relation (Rayleigh–Lamb equation) are determined.

Using elasticity equations, the dispersion relation for a homogeneous isotropic plate has been exhaustively studied by Mindlin (1960). Wave propagation in two- or three-layer (sandwich) isotropic plates has been investigated by Yu (1960), Jones (1964) and Lee and Chang (1979). The frequency spectrum for monoclinic crystal plates has been investigated by Kaul and Mindlin (1962). Baylis and Green (1986a, b) and Baylis (1988) investigated analytical dispersion equations for two- or three-layer transversely isotropic plates. Kapania and Raciti (1989) have given a comprehensive list of references on dispersion relations of layered plates. To our knowledge, no suitable method for solving the exact dispersion relation for laminated anisotropic plates, when an arbitrary number of layers are laminated, has been reported.

As the number of layers increases, the extreme complexities involved in obtaining the exact dispersion equation have placed restrictions on obtaining accurate eigenvalues and

eigenvectors. Even if the dispersion relation is obtained, the highly transcendental nature of it requires robust search techniques in locating roots in the complex plane. This searching is computationally very expensive. To circumvent this difficulty, a combined analytical–approximate method is proposed in this paper. The exact dispersion relation of the layered plate is constructed using the propagator matrix or the layer matrix (see Mal, 1988). Each layer may have orthotropic material properties. Muller's method as given in Conte and Boor (1972) is then used in conjunction with starting initial guesses obtained from an approximate theory. Once the roots are found, the wave functions can be computed through the propagator matrix of each sub-layer.

Several approximate theories have been proposed to derive the dispersion relations in the form of algebraic generalized eigenproblems. The most common ones are plate theories. A list of references on numerous refined theories for homogeneous or laminated media consisting of isotropic or anisotropic materials, can be found in Kapania and Raciti (1989) and Librescu and Reddy (1989). However, plate theories are cumbersome to use and they do not provide accurate eigenvalues which are required for the edge reflection problems. Theories which yield accurate eigenvalues and are computationally very convenient to use are the theories derived through the stiffness method of analysis. Recently, Datta *et al.* (1988) presented an approximate stiffness method applicable to a layered anisotropic plate with an arbitrary number of layers, where each layer may have anisotropic properties. In this method, each layer is divided into several sub-layers. Using cubic interpolation polynomials, the continuity of displacements and tractions at the interfaces between sub-layers was achieved. This method gives very accurate results even at high frequencies. However, this method leads to a more computationally demanding algebraic eigenvalue problem than if only linear interpolation polynomials are employed with only displacement continuity at the interfaces. In the latter case, the high accuracy is lost that is obtained using the former. A compromise between the two methods is a method proposed by Dong and his co-researchers (Dong and Pauley, 1978; Dong and Huang, 1985), which will be denoted as Dong's method, where quadratic interpolation polynomials were used. In the present study, eigenvalues obtained from Dong's method were substituted as initial guesses in Muller's algorithm.

Torvik (1967) treated the free end reflection of a homogeneous isotropic plate by expanding the reflected wave field in wave functions. He determined the amplitudes of modes, approximately, by using a variational principle. Wu and Plunkett (1967) also addressed this problem by using a variational principle method and a residual boundary value minimization method. Gregory and Gladwell (1983) have reported a detailed investigation of symmetric Rayleigh–Lamb wave reflection at the edge of a homogeneous isotropic plate by using the method of projection. However, to our knowledge, free end reflection of anisotropic plates has not been reported.

In this paper, the free end reflection that occurs when a train of waves travelling in the negative x-direction (see Fig. 1) and having only one of the possible wave lengths strikes the edge $x = 0$, is investigated. The reflected field consists of a finite number of propagating

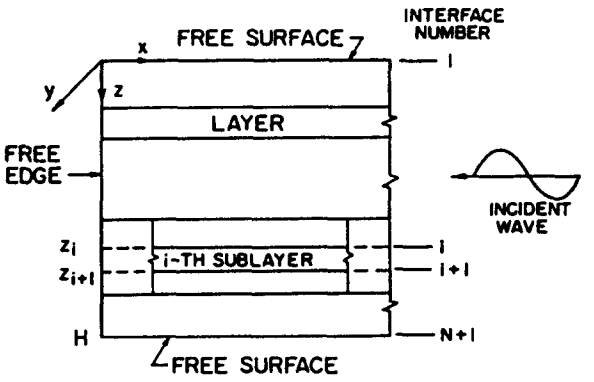

Fig. 1. Geometry of the layered plate.

modes and an infinite number of nonpropagating modes. A finite number of vectors (values of wave functions at discrete number of interfaces) are superposed to represent the reflected field. Amplitudes are determined by satisfying the traction-free edge condition by the least-squares and variational principle methods.

The accuracy of the methods is demonstrated by comparing the results with existing results for a homogeneous isotropic plate. It is shown that for a laminated composite plate, the least-squares method yields anomalous results. Numerical results from the variational method are presented for a single layered graphite/epoxy plate and for a 35-layer cross-ply (90°/0°/.../90°/0°/90°/.../0°/90°) laminated graphite/epoxy plate. In each case, the division of energy among various reflected modes is presented. The end resonance is reported for the single layer graphite/epoxy plate.

2. FORMULATION

Time-harmonic plane strain wave propagation in a semi-infinite plate, composed of perfectly bonded layers with possibly distinct mechanical properties and thickness, is considered. The two faces of the plate $z = 0$ and $z = H$, and edge $x = 0$ are traction free (Fig. 1). For simplicity in analysis, each layer is assumed to be orthotropic. Each layer is divided into several sub-layers so that the total number of sub-layers through the thickness H is N. It should be noted that division into sub-layers is not required to obtain the exact dispersion relation, but is used to compute discrete eigenvectors. A time-harmonic plane strain wave excited at $x = +\infty$, propagates in the plate in the negative x-direction and is incident upon the end $x = 0$.

2.1. *Wave functions*

Wave functions required for the reflection analysis are obtained by considering the plane strain wave propagation in the corresponding infinite plate. Let $u(x, z, t)$, 0, $w(x, z, t)$ denote displacement components in the x, y and z-directions, respectively, and t denote time. Consider the ith sub-layer bounded by $z = z_i$ and $z = z_{i+1}$. The stress–strain relation in this sub-layer is given by

$$\begin{Bmatrix} \sigma_{xx} \\ \sigma_{zz} \\ \sigma_{zx} \end{Bmatrix} = \begin{bmatrix} C_{11} & C_{13} & 0 \\ C_{13} & C_{33} & 0 \\ 0 & 0 & C_{55} \end{bmatrix} \begin{Bmatrix} \varepsilon_{xx} \\ \varepsilon_{zz} \\ \gamma_{zx} \end{Bmatrix}, \tag{1}$$

where σ_{ij} and ε_{ij} are the stress and strain components respectively, and $\gamma_{zx} = 2\varepsilon_{zx}$. C_{ij} are the elements of the constitutive matrix for the sub-layer. The strain components are related to u and w by

$$\varepsilon_{xx} = u_{,x}; \quad \varepsilon_{zz} = w_{,z}; \quad \gamma_{zx} = w_{,x} + u_{,z}; \tag{2}$$

where comma (,) denotes the partial derivative.

In the absence of body forces, within each sub-layer, u and w satisfy the equilibrium equations

$$\begin{aligned} \sigma_{xx,x} + \sigma_{zx,z} &= \rho\ddot{u}, \\ \sigma_{zx,x} + \sigma_{zz,z} &= \rho\ddot{w}, \end{aligned} \tag{3}$$

where ρ is the density of the ith sub-layer and a dot indicates differentiation with respect to time. For plane waves propagating in the x-direction, the appropriate forms for u and w which satisfy eqn (3), are

$$u = jk(\Omega_1^+ + b\Omega_2^+)\exp[j(kx-\omega t)],$$
$$w = (ar_1\Omega_1^- + r_2\Omega_2^-)\exp[j(kx-\omega t)], \tag{4}$$

where

$$\Omega_1^+ = A_{11}\cos r_1 z + A_{12}\sin r_1 z,$$
$$\Omega_1^- = A_{12}\cos r_1 z - A_{11}\sin r_1 z,$$
$$\Omega_2^+ = A_{21}\cos r_2 z + A_{22}\sin r_2 z,$$
$$\Omega_2^- = A_{22}\cos r_2 z - A_{21}\sin r_2 z, \tag{5}$$

$$a = (k_2^2 - \alpha k^2 - r_1^2)/\delta r_1^2,$$
$$b = (k_2^2 - k^2 - \beta r_2^2)/\delta k^2, \tag{6}$$

$$\alpha = \frac{C_{11}}{C_{55}};\quad \beta = \frac{C_{33}}{C_{55}};\quad k_2 = \sqrt{\frac{\rho\omega^2}{C_{55}}};\quad \delta = 1 + \frac{C_{13}}{C_{55}}. \tag{7}$$

k is the wave number, ω is the circular frequency, $j = \sqrt{-1}$ and r_1 and r_2 are the roots of the equation

$$\begin{vmatrix} r^2 + \alpha k^2 - k_2^2 & \delta r^2 \\ \delta k^2 & k^2 - k_2^2 + \beta r^2 \end{vmatrix} = 0. \tag{8}$$

A_{11}, A_{12}, A_{21} and A_{22} are the arbitrary constants for the sub-layer. Stress and displacement components of the sub-layer can be expressed in terms of these four unknown constants. Evaluating the stresses and displacements at $z = z_i$ and $z = z_{i+1}$, after some manipulations, the following relation can be obtained:

$$\mathbf{Q}_{i+1} = [P_i]\mathbf{Q}_i, \tag{9}$$

where

$$\mathbf{Q}_i^T = \langle u_i, w_i, \sigma_{zzi}, \sigma_{zxi}\rangle.$$

The vector quantity $\mathbf{Q}_i$, which is unknown yet, is independent of x and it represents the displacement and stress components at $z = z_i$; superscript T represents the transpose; and $[P_i]$ is the propagator matrix for the ith sublayer. The elements of $[P_i]$ are given in the Appendix.

Repeated application of eqn (9) results in

$$\mathbf{Q}_{N+1} = [P]\mathbf{Q}_1, \tag{10}$$

where

$$[P] = [P_N][P_{N-1}].....[P_2][P_1]. \tag{11}$$

It should be noted that repeated application of eqn (9) ensures the continuity of displacements and stresses at the interfaces. The elements of the 4×4 matrix $[P]$, are denoted by P_{mn} ($m = 1$–4, $n = 1$–4). Invoking the zero traction conditions at interfaces 1 and $(N+1)$, we obtain from eqn (10),

$$\begin{bmatrix} P_{31} & P_{32} \\ P_{41} & P_{42} \end{bmatrix} \begin{Bmatrix} u_1 \\ w_1 \end{Bmatrix} = \begin{Bmatrix} 0 \\ 0 \end{Bmatrix}. \tag{12}$$

Hence, the exact dispersion relation for the plate is given by

$$f(\omega, k) = P_{31}P_{42} - P_{32}P_{41} = 0. \tag{13}$$

For a particular value of ω, eqn (13) will have a finite number of real roots and an infinite number of imaginary and complex roots for k. To express the reflected wave field as a modal sum to satisfy boundary conditions, we superpose all the modes corresponding to the roots with "small" positive imaginary parts as done by Gregory and Gladwell (1983). Let M be the total number of modes to be used in the modal expansion and k_m be the mth root. Traction-free conditions at interface 1 and eqn (12) give the components of the mth eigenvector at interface 1, as

$$\mathbf{Q}_{1m}^{\mathrm{T}} = \langle 1, -P_{31}/P_{32}, 0, 0 \rangle. \tag{14}$$

Then, applying eqn (9) at successive interfaces, the mth mode eigenvector (values of wave function at discrete interfaces) can be obtained as

$$\mathbf{Q}_m^{\mathrm{T}} = \langle \mathbf{Q}_{1m}^{\mathrm{T}}, \mathbf{Q}_{2m}^{\mathrm{T}}, \ldots, \mathbf{Q}_{im}^{\mathrm{T}}, \ldots, \mathbf{Q}_{(N+1)m}^{\mathrm{T}} \rangle, \tag{15}$$

where

$$\mathbf{Q}_{im}^{\mathrm{T}} = \langle u_{im}, \omega_{im}, \sigma_{zzim}, \sigma_{zxim} \rangle, \quad i = 1 \text{ to } N+1; \quad m = 1 \text{ to } M. \tag{16}$$

u_{im}, w_{im}, σ_{zzim} and σ_{zxim} are components of mth eigenvector at the ith interface. The eigenvector $\mathbf{Q}_m$ is normalized by dividing each element through a factor g, defined as

$$g = \sqrt{\sum_{i=1}^{N+1} (u_{im}u_{im}^* + w_{im}w_{im}^*)}. \tag{17}$$

The superscript star (*) refers to the complex conjugate.

If the problem under consideration is symmetric or antisymmetric, it is possible to model only the half-thickness of the plate in the analysis. In this case, the boundary conditions at the middle surface of the plate, $z = H/2$, are:

$$\begin{aligned} w = 0; \quad \sigma_{zx} = 0, \quad &\text{for symmetric problems,} \\ u = 0; \quad \sigma_{zz} = 0, \quad &\text{for antisymmetric problems.} \end{aligned} \tag{18}$$

Applying these boundary conditions in eqn (10), appropriate dispersion relations and eigenvectors can be obtained.

2.2. *Amplitude coefficients*

Consider the case in which the incident wave is the pth propagating mode, corresponding to the wave number k_p. After striking the edge $x = 0$, a reflected wave field will be generated. The displacement vector corresponding to this wave field, $\mathbf{q}_x^r$, at arbitrary x, can be approximated by the modal sum of a finite number of modes M in the form

$$\mathbf{q}_x^r = \sum_{m=1}^{M} B_m \mathbf{q}_m \exp(\mathrm{j}k_m x); \quad x \geqslant 0, \tag{19}$$

where

$$B_m = \text{amplitude of } m\text{th reflected mode},$$

$$\mathbf{q}_m^{\mathrm{T}} = \langle u_{1m}, w_{1m}, \ldots, u_{im}, w_{im}, \ldots, u_{(N+1)m}, w_{(N+1)m} \rangle. \tag{20}$$

Equation (19) gives the reflected wave field at the edge $x = 0$ as

$$\mathbf{q}_0^{\mathrm{r}} = [G]\mathbf{B}, \tag{21}$$

where

$$[G] = [\mathbf{q}_1, \mathbf{q}_2, \ldots, \mathbf{q}_M], \tag{22}$$

$$\mathbf{B}^{\mathrm{T}} = \langle B_1, B_2, \ldots, B_M \rangle. \tag{23}$$

By solving eqns (1), (2) and (4), the σ_{xx} components of stresses within the ith sub-layer can be obtained as

$$\sigma_{xx} = \frac{C_{55}}{\Delta_1}[C_{55}(de - cf)u + jk(f - be)\sigma_{zz}], \tag{24}$$

where

$$e = (1-\delta)ar_1^2 - \alpha k^2, \tag{25}$$

$$f = (1-\delta)r_2^2 - \alpha k^2 h, \tag{26}$$

and c, d and Δ_1 are defined in the Appendix. Since u_{im} and σ_{zzim} for the mth mode are known from eqn (15), eqn (24) can be used to compute σ_{xxim} at each interface. It should be noted that σ_{xx} is discontinuous at the interfaces between layers. The force vector at the edge due to the reflected field can now be formed as

$$\mathbf{R}^{\mathrm{r}} = -[F]\mathbf{B}, \tag{27}$$

where $[F]$ is the force mode shape matrix which represents the nodal force mode shapes at the interfaces, due to stresses σ_{xx} and σ_{xz}. $[F]$ is a rectangular matrix of size $2(N+1)$ by M. In constructing the force vector, the consistent load vector formulation given in Bathe (1982) has been used. The variation of displacements and stresses within the sub-layer is assumed to be linear. The explicit form of $[F]$ is given in the Appendix.

The edge force vector due to incident field can be written as

$$\mathbf{R}^{\mathrm{in}} = A_p^{\mathrm{in}}\mathbf{F}_p^-, \tag{28}$$

where A_p^{in} is the amplitude of the incident mode and the vector $\mathbf{F}_p^-$ is obtained from the pth column of $[F]$, after replacing each x-direction force component by the negative value of it.

The traction-free edge condition requires that

$$\mathbf{R} = \mathbf{R}^{\mathrm{r}} + R^{\mathrm{in}} = -[F]\mathbf{B} + A_p^{\mathrm{in}}\mathbf{F}_p^- = \mathbf{0}. \tag{29}$$

Subjecting the sum of the squares of the residuals of $\mathbf{R}$ to a least-squares minimization, the least-squares solution for complex amplitude coefficients can be obtained as

$$\mathbf{B} = A_p^{\mathrm{in}}[[F^*]^{\mathrm{T}}[F]]^{-1}[F^*]^{\mathrm{T}}\mathbf{F}_p^-. \tag{30}$$

A variational solution to the problem can be obtained by applying the principle of virtual displacement as in Wu and Plunkett (1967). This results in

$$\delta \mathbf{q}^{*\mathrm{T}} \mathbf{R} = \mathbf{0}, \tag{31}$$

where δ implies variation. It may be noted that the total displacement field, $\mathbf{q}$, at $x = 0$ is given by

$$\mathbf{q} = \mathbf{q}_0^{\mathrm{r}} + \mathbf{q}_0^{\mathrm{in}} \tag{32}$$

and

$$\delta \mathbf{q} = \delta \mathbf{q}_0^{\mathrm{r}}, \tag{33}$$

where $\mathbf{q}_0^{\mathrm{in}}$ is the incident field.

Substituting eqns (29) and (33) in eqn (31), and making use of eqn (21), the variational form of the solution is obtained as

$$\mathbf{B} = A_p^{\mathrm{in}} [[G^*]^{\mathrm{T}} [F]]^{-1} [G^*]^{\mathrm{T}} \mathbf{F}_p^-. \tag{34}$$

We define the normalized amplitude A_m by

$$A_m = B_m / A_p^{\mathrm{in}}. \tag{35}$$

Once the amplitudes, B_m, are known, the displacement and stress field anywhere in the plate can be computed.

2.3. *Energy flux*

Reflected energy is carried only by the propagating modes. The time-average value of the energy flux associated with the jth reflected propagating mode through the plate cross-section, is given by

$$I_j^{\mathrm{r}} = \omega |B_j|^2 J_j; \quad j \leqslant N_{pr}, \tag{36}$$

where

$$J_j = \mathrm{Im}\,[\mathbf{F}_j^{\mathrm{T}} \cdot \mathbf{q}_j^*]. \tag{37}$$

In eqn (36), N_{pr} represents the number of propagating modes in the reflected field. Similarly, the energy flux of the incident wave can be written as

$$I_p^{\mathrm{in}} = \omega |A_p^{\mathrm{in}}|^2 \,\mathrm{Im}\,[(\mathbf{F}_p^-)^{\mathrm{T}} \cdot (\mathbf{q}_p^-)^*], \tag{38}$$

where $\mathbf{q}_p^-$ is the pth column of $[G]$, after replacing each x-direction displacement components by the negative value of it.

Let E_j be the proportion of incident energy transferred into the jth reflected mode, then

$$E_j = I_j^{\mathrm{r}} / I_p^{\mathrm{in}}. \tag{39}$$

Another useful index is the percentage error in energy balance, ε, defined by

$$\varepsilon = \left[I_p^{\mathrm{in}} - \sum_{n=1}^{N_{pr}} I_j^{\mathrm{r}} \right] 100 / I_p^{\mathrm{in}}. \tag{40}$$

The principle of energy conservation requires that sum E_j be unity, namely ε should be zero. This condition is used to assess the accuracy of our analysis.

3. NUMERICAL RESULTS AND DISCUSSION

In this section, the numerical algorithm employed for the evaluation of the roots of the dispersion relation (13) and the numerical results of the reflection problem for four examples are presented.

3.1. *Wave number determination*

For a fixed value of the frequency ω, eqn (13) is a transcendental function of the wave number, k. As reported by Torvik (1967) and Gregory and Gladwell (1983), the admissible k for the reflected wave field of the semi-infinite plate are those real roots with positive group velocity and those non-real roots with $\mathrm{Im}(k) > 0$. These conditions ensure that the reflected waves produce bounded displacement and stress fields throughout the plate. It is possible to find the roots of eqn (13) by a brute-force method, or a gradient search method in a complex wave number plane as described in Press *et al.* (1988). This approach will be computationally formidable since the roots are sparsely scattered in the complex k-plane.

Herein, Muller's method is employed. At the first step, beginning with the highest frequency of interest, the plate is divided into a sufficiently large number of sub-layers and the approximate roots are obtained via Dong's method, using an IMSL (1984) sub-routine for standard algebraic eigenvalue problems. Those approximate roots lying in the first quadrant of the complex k-plane, are used as initial guesses in Muller's method to recover the exact roots. At the next step, ω is decreased by a small amount and eqn (13) is solved, taking exact roots from the previous step as initial guesses for the current step. The process is repeated until the frequency range of interest is scanned. As a check, at some intermediate frequencies, approximate roots from Dong's method were used as initial guesses in Muller's method to obtain exact roots. After obtaining the wave numbers k, for the frequency range of interest, the signs of the real wave numbers were adjusted to have positive group velocities. M number of roots k, are ordered as follows: real roots are ordered first in decreasing order of magnitude. Non-real roots are ordered next in the ascending order of magnitude of their imaginary parts. Whenever a complex root k, which is not purely imaginary is encountered, the negative complex conjugate, $-k^*$, is also included.

3.2. *Numerical examples*

The following four numerical examples were considered:

Example 1—a homogeneous isotropic plate with Poisson's ratio, $\nu = 0.25$. The incident wave considered is the first symmetric propagating mode.

Example 2—a homogeneous graphite/epoxy (transversely isotropic) plate with fibers aligned along the x-axis (0°). See Table 1 for material properties. The incident wave is the first symmetric propagating mode.

Example 3—a 35-layer graphite/epoxy cross-ply laminated plate with 90°/0°/.../90°/0°/90/.../0°/90° configuration. Material properties are given in Table 1. The incident wave is the first symmetric propagating mode.

Example 4—same as in example 3, but the incident wave is the first antisymmetric propagating mode.

Since in each of the above examples, the problem is either symmetric of antisymmetric, only the half-thickness of the plate was considered in the analysis. In all four examples, the

Table 1. Elastic properties of 0° and 90° graphite/epoxy fibers. All stiffnesses are in units of 10^{11} Nm^{-2}

lamina	C_{11}	C_{33}	C_{13}	C_{55}
0° lamina	1.6073	0.1392	0.0644	0.0707
90° lamina	0.1392	0.1392	0.0692	0.0350

real branches of the frequency spectrum were plotted to identify the positive group velocity zones. Figure 2 shows the frequency spectrum for examples 2–4. The following non-dimensionalization is used for frequency and wave number throughout this section:

$$\text{Example 1}—\Omega = \frac{\omega H}{2c_d\sqrt{\mu/\rho}}, \quad \gamma = \frac{1}{2}kH,$$

$$\text{where} \quad c_d = \sqrt{\frac{3\mu}{\rho}}, \quad \mu = \text{shear modulus}.$$

$$\text{Examples 2–4}—\Omega = \frac{\omega H}{2\sqrt{(C_{55}/\rho)_0}}, \quad \gamma = \frac{1}{2}kH.$$

The total number of sub-layers N, used to compute the eigenvectors and the number of modes M used in the modal expansion, plays an important role in the accuracy of our method. In order to select a suitable value for N, the quantity $J_j (j = 1 \text{ to } N_{pr})$ defined in eqn (37) was computed by increasing the value of N at a few selected lower, intermediate and higher frequencies in the frequency range of interest, until convergent values were obtained for J_j. In this way, reasonably good values for N through the half-thickness were found to be 50 in examples 1 and 2, and 70 in examples 3 and 4. Thereafter, the reflection problem was solved at the selected frequencies by the least-squares method [eqn (30)] and by the variational method [eqn (34)], by increasing the number of modes. Tables 2 and 3 show some of the results obtained from two methods for percentage error in energy balance ε, and the modulus of the amplitude of the first reflected mode, $|A_1|$. In example 1 at $\Omega = 4.0$, the reflected field consists of four symmetric propagating modes; in example 2 at $\Omega = 4.0$,

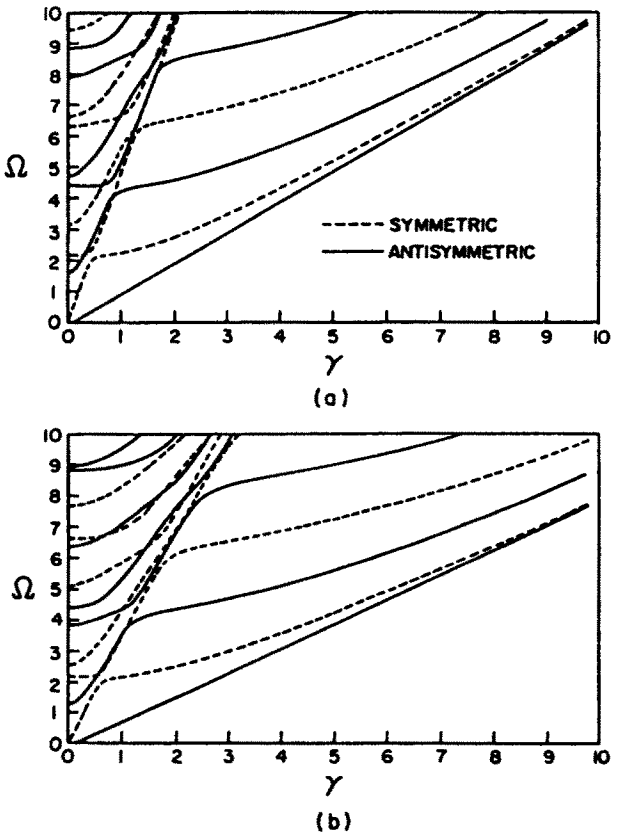

Fig. 2. Real branches of the frequency spectrum. (a) Homogeneous graphite/epoxy plate. (b) 35-layer cross-ply (90°/0°/,...,/90°/0°/90°/,...,/0°/90°) graphite/epoxy plate.

Table 2. Variation of percentage error ε in energy balance and amplitude modulus $|A_1|$ with M number of modes for homogeneous plate

Example	M	ε		$\lvert A_1 \rvert$	
		Eq. (30)	Eq. (34)	Eq. (30)	Eq. (34)
Example 1 $\Omega = 4.0$	4	51.354	10.836	0.170	0.245
	7	21.505	1.907	0.339	0.426
	11	3.192	0.062	0.477	0.493
	15	0.982	0.073	0.489	0.494
	19	0.325	0.140	0.493	0.494
	21	0.209	0.153	0.493	0.494
	23	0.155	0.160	0.494	0.494
	25	0.127	0.164	0.494	0.494
Example 2 $\Omega = 4.0$	3	76.231	17.229	0.122	0.590
	6	58.006	7.023	0.253	0.621
	8	44.888	5.915	0.371	0.623
	12	9.112	0.654	0.665	0.704
	15	6.423	0.830	0.680	0.704
	20	2.068	0.247	0.696	0.708
	25	1.212	0.223	0.702	0.709
	29	0.499	0.195	0.705	0.709

Table 3. Variation of percentage error ε in energy balance and amplitude $|A_1|$ with M number of modes for 35-layer graphite/epoxy plate

Example	M	ε		$\lvert A_1 \rvert$	
		Eq. (30)	Eq. (34)	Eq. (30)	Eq. (34)
Example 3 $\Omega = 5.1$	3	91.947	28.291	0.188	0.735
	6	91.946	19.259	0.162	0.772
	10	92.265	19.892	0.109	0.807
	12	84.150	16.481	0.102	0.741
	15	70.368	4.019	0.270	0.796
	18	54.948	1.669	0.436	0.807
	21	53.912	0.296	0.440	0.812
	24	54.996	0.172	0.441	0.811
	27	51.559	0.005	0.476	0.809
	30	51.519	-0.001	0.477	0.809
Example 4 $\Omega = 4.0$	3	89.365	13.817	0.083	0.674
	6	75.730	11.045	0.242	0.776
	10	74.344	9.437	0.330	0.786
	12	63.389	6.579	0.469	0.803
	15	59.559	4.778	0.511	0.814
	17	23.118	1.466	0.776	0.827
	21	20.463	0.487	0.791	0.831
	24	20.471	0.388	0.792	0.831
	27	20.474	0.362	0.792	0.831

the reflected field consists of three symmetric propagating modes; in example 3 at $\Omega = 5.1$, the reflected field consists of three symmetric propagating modes; and in example 4 at $\Omega = 4.0$, the reflected field consists of three antisymmetric propagating modes. Comparison of the results from the two methods shows that the variational method gives very good energy balance and convergence of the amplitude $|A_1|$, even with a relatively smaller number of modes. It can be noticed that for the homogeneous plate, there is no noticeable difference in the results from the two methods if a sufficiently large number of modes are taken. For

the laminated plate, the results obtained by the least-squares method are alarming. Even with 30 modes participation, only 50% of the incident mode energy is reflected back into the plate from the free edge for symmetric incidence, which is an anomaly. The reason for this anomaly is obvious. Unlike the variational method which minimizes the energy, the least-squares method does not have a physical basis. In the least-squares method, even though the sum of the squares of the residuals in **R** is minimized, the minimized residual sum could be large resulting in large errors in ε. In what follows, only the results obtained from the variational method are presented.

Figure 3 shows the comparison of proportion of energy E_j obtained by the present method with those of Gregory and Gladwell (1983) for an isotropic plate. The modal expansion consisted of 21 modes. For the range of Ω in Fig. 3, $|\varepsilon| < 0.18\%$; it is seen that the comparison is excellent. Even though the results for amplitude $|A_1|$ are not presented here due to space limitations, our results were in complete agreement with those of Gregory and Gladwell (1983). A full discussion on the energy distribution among reflected modes for this case can be found in Gregory and Gladwell (1983).

The energy distribution among various reflected propagating modes in example 2 is shown in Fig. 4. The modal expansion consisted of 20 modes. For the range $0 < \Omega < 2.196$ (which is not shown in Fig. 4), $|\varepsilon|$ was less than 0.05%. For the range of results presented here, $|\varepsilon| < 0.88\%$. The range $2.197 < \Omega \leqslant 2.2041$ is the backward-wave transmission region discussed by Meitzler (1965), where the third propagating mode has a negative phase velocity. In particular, it was observed that at the first cut-off $\Omega = 2.2041$, only the second mode carries energy; at the second cut-off $\Omega = 3.142$, only the first mode carries energy; at the third cut-off $\Omega = 6.283$, all three modes carry energy and in the range $2.4 < \Omega < 5.9$, the first and third modes share almost the entire reflected energy. In Fig. 5(a), the variation of amplitude $|A_1|$ with Ω is shown. It can be seen that $|A_1| = 1.0$ in the range $0 < \Omega < 2.197$. Since only one propagating mode exists in this frequency range, the entire energy is reflected into the first mode, and therefore, by the energy conservation principle, $|A_1|$ has to be equal to unity. For $\Omega > 2.197$, $|A_1|$ is oscillatory. After a careful search, it was noted that edge resonance occurs in the second mode near $\Omega = 2.1520$. The variation of amplitude $|A_2|$ near resonant frequency is shown in Fig. 5(b). At $\Omega = 2.1520$, by increasing M from 20 to 30, ε changed from 0.14% to 0.01% and only a 0.11% increase in $|A_2|$ was observed.

The division of energy between various reflected modes for examples 3 and 4 is presented in Figs 6 and 7 respectively. Figures 8(a) and 8(b) show amplitude $|A_1|$, for examples 3 and 4 respectively. The first three cut-off frequencies are $\Omega = 2.204$, 2.556 and 5.111 for symmetric modes, and $\Omega = 1.278$, 3.834 and 4.408 for antisymmetric modes. The symmetric case consisted of 22 modes whilst in the antisymmetric case, 21 modes were used. In the frequency ranges considered, $|\varepsilon| < 0.44\%$ for the symmetric case and $|\varepsilon| < 0.18\%$ for the antisymmetric case. In particular, it is seen from Figs 6(b) and 7 that between the second and third cut-off frequencies, in the symmetric case, energy is shared almost entirely between the first and third modes, whereas in the antisymmetric case, energy is shared among all three modes. A careful search was made for the end resonance frequency in the symmetric case but none could be found and therefore, no search was made for the antisymmetric case.

4. CONCLUSION

A semi-analytical method employing exact discrete eigenvectors for displacements and stresses has been used to study the guided plane strain wave reflection at the free edge of a laminated composite plate. Problems were solved by the least-squares method and the variational method. It was found that the variational method gave very good results. It was shown that the results agree well with known solutions for homogeneous isotropic plates. Since the exact eigenvectors were employed, the method was accurate at both low frequencies and high frequencies. Since the least-squares method gave anomalous results from the point of view of energy balance, it is concluded that the method should not be used for the free end reflection problem of layered plates. Although the case of wave propagation

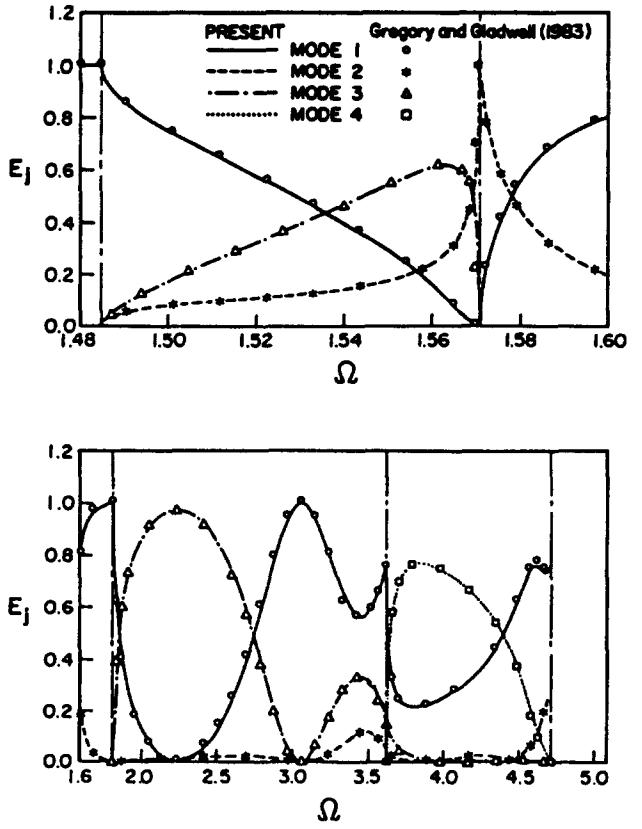

Fig. 3. The proportions of energy E_j for the homogeneous isotropic plate due to the first symmetric incident mode ($\nu = 0.25$).

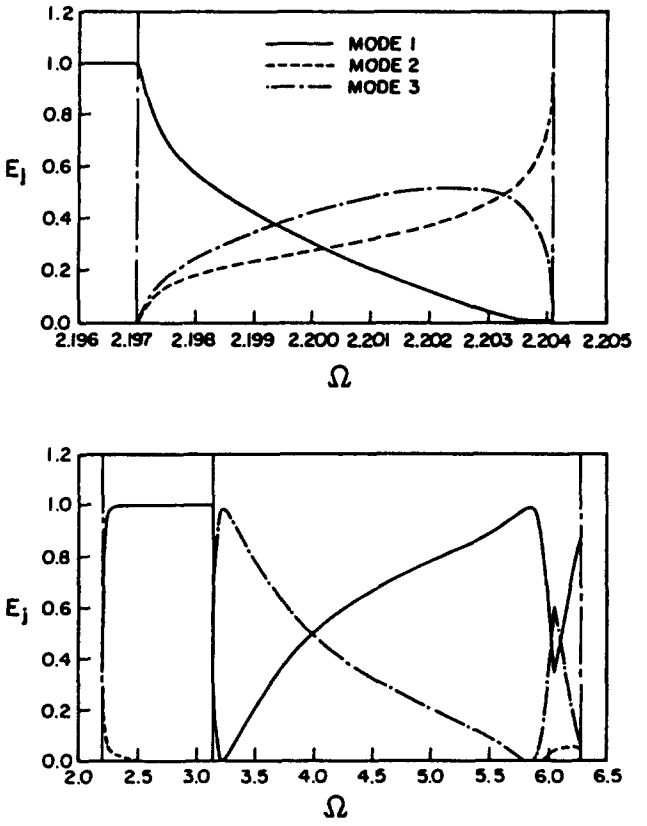

Fig. 4. The proportions of energy E_j for the homogeneous graphite/epoxy plate due to the first symmetric incident mode.

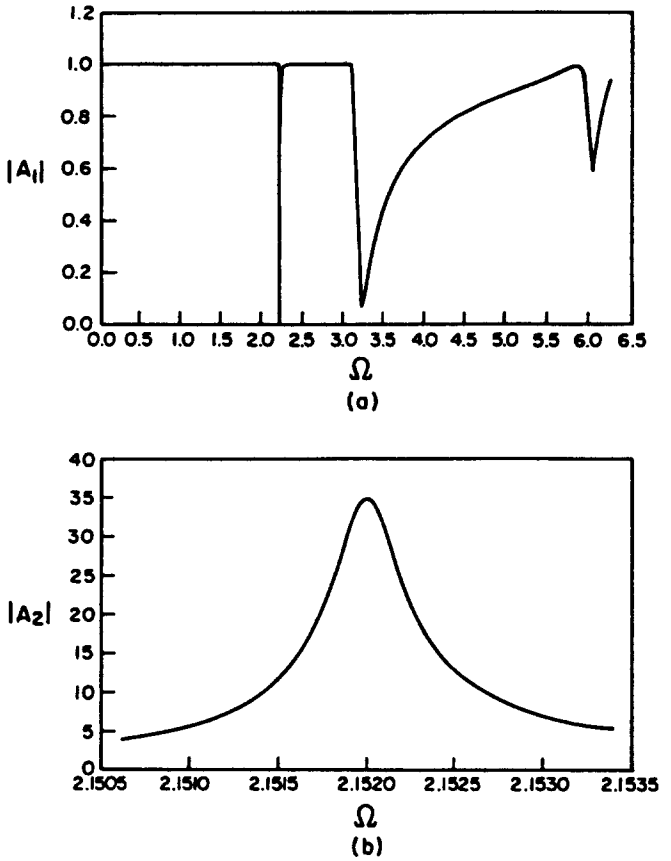

Fig. 5. The amplitude $|A_j|$ for the homogeneous graphite/epoxy plate due to the first symmetric incident mode. (a) Amplitude $|A_1|$, (b) amplitude $|A_2|$.

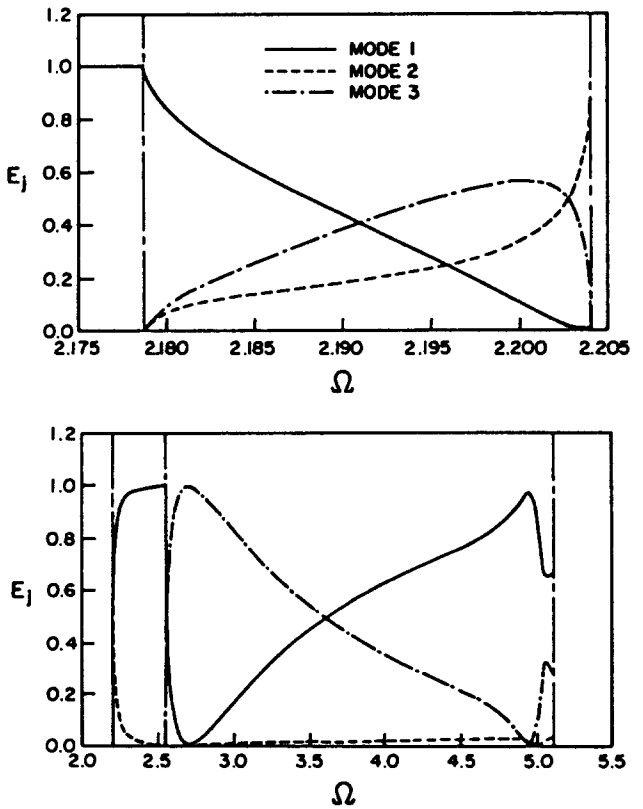

Fig. 6. The proportions of energy E_j for the 35-layer graphite/epoxy plate due to the first symmetric incident mode.

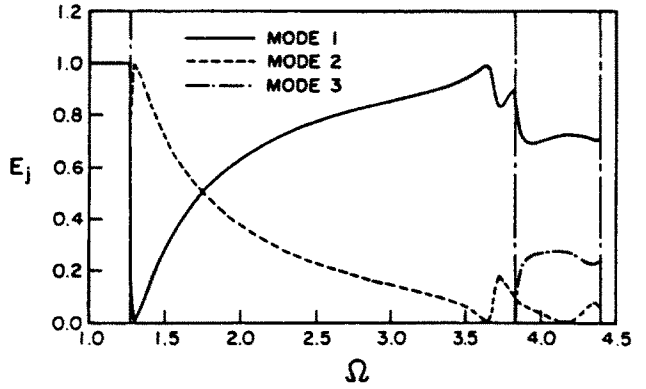

Fig. 7. The proportions of energy E_j for the 35-layer graphite/epoxy plate due to the first antisymmetric incident mode.

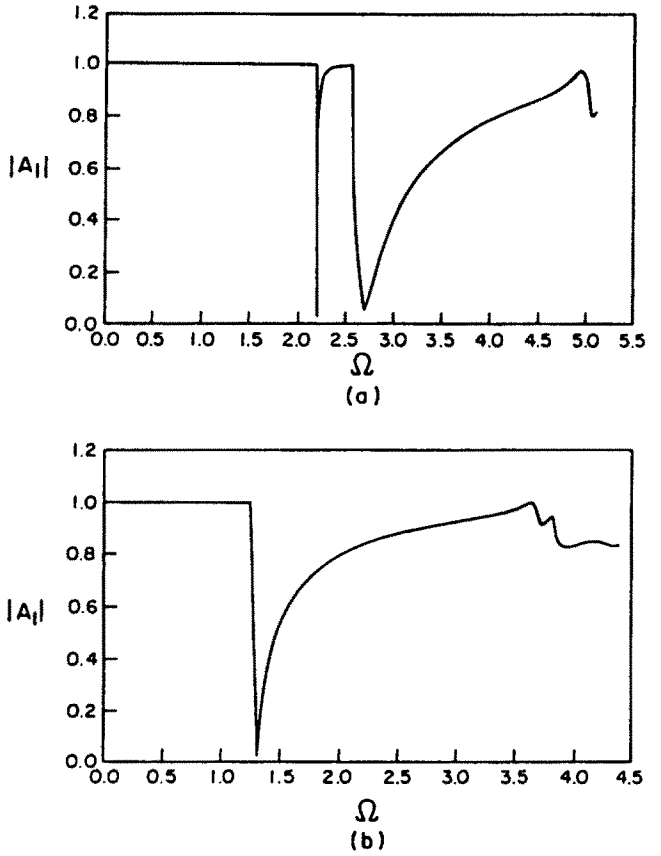

Fig. 8. The amplitude $|A_1|$ for the 35-layer graphite/epoxy plate, (a) due to first symmetric incident mode, (b) due to first antisymmetric incident mode.

along a principle direction has been studied, the method is easily applicable to off-axis propagation.

Acknowledgements—This work was supported by a grant from the Natural Science and Engineering Council of Canada (0GP-0007988). Partial support was also received from the Office of Naval Research (# N00014-86-K-0280; Program Manager: Dr Y. Rajapakse).

REFERENCES

Abduljabbar, Z., Datta, S. K. and Shah, A. H. (1983). Diffraction of horizontally polarized shear waves by normal edge cracks in a plate. *J. Appl. Phys.* 54(2), 461–472.

Bathe, K. J. (1982). *Finite Element Procedures in Engineering Analysis*. Prentice-Hall, New Jersey.
Baylis, E. R. (1988). Wave propagation in asymmetric fibre-reinforced laminated plate, Part II. *Acta Mechanica* **71**, 167–183.
Baylis, E. R. and Green, W. A. (1986a). Flexural waves in fibre-reinforced laminated plates. *J. Sound Vibr.* **110**(1), 1–26.
Baylis, E. R. and Green, W. A. (1986b). Flexural waves in fibre-reinforced laminated plates, Part II. *J. Sound Vibr.* **111**(2), 181–190.
Conte, S. D. and Boor, C. D. (1972). *Elementary Numerical Analysis*, 2nd Edn. McGraw-Hill, New York.
Datta, S. K., Bratton, R. L., Chakraborthy, T. and Shah, A. H. (1988). Wave propagation in laminated composite plates. *J. Acoust. Soc. Am.* **83**, 2020–2026.
Dong, S. B. and Huang, K. H. (1985). Edge vibrations in laminated composite plates. *J. Appl. Mech.* **52**, 433–438.
Dong, S. B. and Pauley, K. E. (1978). Plane waves in anisotropic plates. *J. Engng Mech. Div. ASCE* **104**, 801–817.
Gregory, R. D. and Gladwell, I. (1983). The reflection of a symmetric Rayleigh–Lamb wave at the fixed or free edge of a plate. *J. Elast.* **13**, 185–206.
International Mathematical and Statistical Libraries Inc. (1984). *IMSL Library*. Houston, Texas.
Jones, J. P. (1964). Wave propagation in two-layered medium. *J. Appl. Mech.* **31**, 213–222.
Kapania, R. K. and Raciti, S. (1989). Recent advances in analysis of laminated beams and plates, Part II: Vibrations and wave propagation. *AIAA Jl* **27**(7), 935–946.
Kaul, R. K. and Mindlin, R. D. (1962). Frequency spectrum of a monoclinic crystal plate. *J. Acoust. Soc. Am.* **34**, 1902–1910.
Lee, P. C. Y. and Chang, N. (1979). Harmonic waves in elastic sandwich plates. *J. Elast.* **9**(1), 51–69.
Librescu, L. and Reddy, J. N. (1989). A few remarks concerning several refined theories of anisotropic composite laminated plates. *Int. J. Engng Sci.* **27**(5), 515–527.
Mal, A. K. (1988). Wave propagation in layered composite laminates under periodic surface loads. *Wave Motion* **10**, 257–266.
Meitzler, A. H. (1965). Backward-wave transmission of stress pulses in elastic cylinders and plates. *J. Acoust. Soc. Am.* **38**, 835–842.
Mindlin, R. D. (1960). Waves and vibrations in isotropic, elastic solids. *Proc. 1st Symp. Naval Structural Mechanics* (Edited by J. N. Goodier and N. Noff), pp. 199–232. Pergamon Press, Oxford, U.K.
Press, W. H., Flannery, B. P., Teukolsky, S. A. and Wetterling, W. T. (1988). *Numerical Recipes*. Cambridge University Press, U.K.
Torvik, P. J. (1967). Reflection of wave trains in semi-infinite plates. *J. Acoust. Soc. Am.* **41**, 346–353.
Wu, C. H. and Plunkett, R. (1967). On the solutions of plates, strips, rods and cylinders subjected to arbitrary dynamic edge load. *SIAM J. Appl. Math.* **15**, 107–119.
Yu, Y. Y. (1960). Forced flexural vibrations of elastic sandwich plate. *J. Appl. Mech.* **27**, 535–540.

APPENDIX

The elements of the propagator matrix $[P_i]$ appearing in eqn (9) are given below

$$[P_i] = \begin{bmatrix} p_{11} & p_{12} & p_{13} & p_{14} \\ p_{21} & p_{22} & p_{23} & p_{24} \\ p_{31} & p_{32} & p_{33} & p_{34} \\ p_{41} & p_{42} & p_{43} & p_{44} \end{bmatrix}; \tag{A1}$$

where

$$p_{11} = \frac{C_{55}}{\Delta_1} jk[d\cos(r_1 h) - cb\cos(r_2 h)],$$

$$p_{21} = \frac{C_{55}}{\Delta_1}[-r_1 ad\sin(r_1 h) + r_2 c\sin(r_2 h)],$$

$$p_{31} = \frac{C_{55}^2}{\Delta_1} cd[\cos(r_1 h) - \cos(r_2 h)],$$

$$p_{41} = \frac{C_{55}^2}{\Delta_1} jk[-r_1 d(1+a)\sin(r_1 h) + r_2 c(1+b)\sin(r_2 h)],$$

$$p_{12} = \frac{C_{55}}{\Delta_2} k^2[-r_2(1+b)\sin(r_1 h) + br_1(1+a)\sin(r_2 h)],$$

$$p_{22} = \frac{C_{55}}{\Delta_2} jkr_1 r_2[a(1+b)\cos(r_1 h) - (1+a)\cos(r_2 h)],$$

$$p_{32} = \frac{C_{55}^2}{\Delta_2} jk[cr_2(1+b)\sin(r_1 h) - dr_1(1+a)\sin(r_2 h)],$$

$$p_{42} = \frac{C_{55}^2}{\Delta_2} k^2 r_1 r_2(1+a)(1+b)[-\cos(r_1 h) + \cos(r_2 h)],$$

$$p_{13} = \frac{bk^2}{\Delta_1}[\cos(r_1 h) - \cos(r_2 h)],$$

$$p_{23} = \frac{jk}{\Delta_1}[r_1 ab \sin(r_1 h) - r_2 \sin(r_2 h)],$$

$$p_{33} = \frac{C_{55}}{\Delta_1} jk[-bc\cos(r_1 h) + d\cos(r_2 h)],$$

$$p_{43} = \frac{C_{55}}{\Delta_1} k^2[-r_1 b(1+a)\sin(r_1 h) + r_2(1+b)\sin(r_2 h)],$$

$$p_{14} = \frac{jk}{\Delta_2}[-r_2 \sin(r_1 h) + abr_1 \sin(r_2 h)],$$

$$p_{24} = \frac{a}{\Delta_2} r_1 r_2[-\cos(r_1 h) + \cos(r_2 h)],$$

$$p_{34} = \frac{C_{55}}{\Delta_2}[-r_2 c \sin(r_1 h) + r_1 ad \sin(r_2 h)],$$

$$p_{44} = \frac{C_{55}}{\Delta_2} jkr_1 r_2[-(1+a)\cos(r_1 h) + a(1+b)\cos(r_2 h)], \tag{A2}$$

$$c = (1-\delta)k^2 - \beta r_1^2 a,$$

$$d = (1-\delta)k^2 b - \beta r_2^2,$$

$$\Delta_1 = C_{55} jk\beta r_2^2 \left(\frac{r_1^2}{r_2^2} ab - 1\right),$$

$$\Delta_2 = C_{55} jkr_1 r_2 (ab - 1),$$

$$h = z_{i+1} - z_i = h_i. \tag{A3}$$

The explicit form of the $[F]$ matrix introduced in eqn (27) is as follows:

$$[F] = [\mathbf{F}_1, \mathbf{F}_2, \ldots, \mathbf{F}_m, \ldots, \mathbf{F}_M]; \tag{A4}$$

where

$$\mathbf{F}_m^{\mathrm{T}} = \langle F_{1m}^x, F_{1m}^z, \ldots, F_{im}^x, F_{im}^z, \ldots, F_{(N+1)m}^x, F_{(N+1)m}^z \rangle, \tag{A5}$$

$$F_{1m}^x = \frac{h_1}{6}(2\sigma_{x\,1m} + \sigma_{x\,2m}^{(-)}),$$

$$F_{1m}^z = \frac{h_1}{6}(2\sigma_{z\,1m} + \sigma_{z\,2m}),$$

$$F_{im}^x = \frac{h_{i-1}}{6}(\sigma_{x(i-1)m}^{(+)} + 2\sigma_{x\,im}^{(-)}) + \frac{h_i}{6}(2\sigma_{x\,im}^{(+)} + \sigma_{x(i+1)m}^{(-)}) \quad \text{for } 2 \leqslant i \leqslant N,$$

$$F_{im}^z = \frac{h_{i-1}}{6}(\sigma_{z(i-1)m} + 2\sigma_{z\,im}) + \frac{h_i}{6}(2\sigma_{z\,im} + \sigma_{z(i+1)m}) \quad \text{for } 2 \leqslant i \leqslant N,$$

$$F_{(N+1)m}^x = \frac{h_N}{6}(\sigma_{x\,Nm}^{(+)} + 2\sigma_{x(N+1)m}),$$

$$F_{(N+1)m}^z = \frac{h_N}{6}(\sigma_{z\,Nm} + 2\sigma_{z(N+1)m}). \tag{A6}$$

In eqn (A6), $\sigma_{x\,im}^{(+)}$ and $\sigma_{x\,im}^{(-)}$ $(2 \leqslant i \leqslant N)$ denote the mth mode normal stresses in the x-direction, just above and below the ith interface, respectively. If the adjacent sub-layers of the ith interface have the same material properties, $\sigma_{x\,im}^{(+)}$ will be equal to $\sigma_{x\,im}^{(-)}$.